THE JOURNAL OF BIOLOGICAL CHEMISTRY
Vol. 277, No. 42, Issue of October 18, pp. 39873–39879, 2002

Printed in U.S.A.

Characterization of Aquaporin-6 as a Nitrate Channel in Mammalian Cells

REQUIREMENT OF PORE-LINING RESIDUE THREONINE 63*

Received for publication, July 12, 2002, and in revised form, August 4, 2002
Published, JBC Papers in Press, August 9, 2002, DOI 10.1074/jbc.M207008200

Masahiro Ikeda‡§, Eric Beitz§¶‖, David Kozono¶, William B. Guggino‡, Peter Agre¶, and Masato Yasui¶‡‡§§**

*From the Departments of ‡Physiology, ¶Biological Chemistry, **Medicine, and ‡‡Pediatrics, Johns Hopkins University School of Medicine, Baltimore, Maryland 21205*

Aquaporins (AQP) were originally regarded as plasma membrane channels that are freely permeated by water or small uncharged solutes but not by ions. Unlike other aquaporins, AQP6 overexpressed in *Xenopus laevis* oocytes was previously found to exhibit Hg^{2+} or pH-activated ion conductance. AQP6 could not be analyzed electrophysiologically in mammalian cells, however, because the protein is restricted to intracellular vesicles. Here we report that addition of a green fluorescence protein (GFP) tag to the N terminus of rat AQP6 (GFP-AQP6) redirects the protein to the plasma membranes of transfected mammalian cells. This permitted measurement of rapid, reversible, pH-induced anion currents by GFP-AQP6 in human embryonic kidney 293 cells. Surprisingly, anion selectivity relative to Cl^- revealed high nitrate permeability even at pH 7.4; $P_{NO_3}/P_{Cl} > 9.8$. Site-directed mutation of a pore-lining threonine to isoleucine at position 63 at the midpoint of the channel reduced NO_3^-/Cl^- selectivity. Moreover, no anomalous mole-fraction behavior was observed with NO_3^-/Cl^- mixtures, suggesting a single ion-binding pore in each subunit. Our studies indicate that AQP6 exhibits a new form of anion permeation with marked specificity for nitrate conferred by a specific pore-lining residue, observations that imply that the primary role of AQP6 may be in cellular regulation rather than simple fluid transport.

Aquaporin water channels are found in all forms of life, with at least 11 members of the family being expressed in mammals. Most characterized mammalian aquaporins are localized to plasma membranes where they mediate the cellular entry or release of water (aquaporins) or glycerol and small neutral solutes (aquaglyceroporins) (1). Aquaporin-6 (AQP6)[1] is unlike other members of the aquaporin family in terms of distribution and function. AQP6 resides exclusively in the membranes of intracellular vesicles of acid-secreting intercalated cells in renal collecting duct where it colocalizes with H^+-ATPase (2, 3). AQP6 expression is increased in rat models of chronic alkalosis or lithium-induced nephrogenic diabetes insipidus, but the cellular distribution of AQP6 is not altered (4). Restriction of AQP6 to intracellular vesicles may be critical for its physiological function.

It is widely believed that most aquaporins are virtually impermeable to ions (5). Several recent studies have revealed high resolution atomic structures of aquaporins (6–8). The atomic structure of AQP1 provided insight into the lack of ion permeability, a feature that is essential for answering the longstanding question of how membranes can be freely permeated by water but impermeable to protonated water, H_3O^+ (6). Molecular dynamics simulations based on the atomic structures have shown ultra high speed movement of water molecules through the aqueous pore in each subunit of the aquaporin tetramer (9, 10). These studies demonstrated that a highly conserved, pore-lining arginine forms a proton-repelling selectivity filter at a critical narrowing in the channel. It was also demonstrated that reorientation of the dipole is needed for simultaneous hydrogen bonding of an isolated water molecule to two perfectly conserved pore-lining asparagines in the signature motifs Asn-Pro-Ala, thereby creating a block in the center of the membrane to the movement of protons along the single file column of water (11).

Unlike other aquaporins, AQP6 was found to be permeated by anions in response to acidic pH or Hg^{2+} activation (3). Moreover, Hg^{2+}-activated ion conductance has been verified by single-channel recordings of oocytes expressing AQP6 (12). The number of Hg^{2+}-binding sites and the kinetics of Hg^{2+} activation of the channel indicate that each subunit of the AQP6 tetramer has an individual ion-conducting pore (12). In contrast, it has been suggested that a single ion-conducting pathway resides at the 4-fold axis in the center of the homotetramer in the *Escherichia coli* aquaglyceroporin, GlpF (7). A putative channel at the 4-fold axis may explain the rare and aberrant membrane currents sometimes observed with AQP1 (13, 14). Nevertheless, it is still uncertain how ions pass though AQP6.

In this study we sought to investigate the activation and anion selectivity of AQP6 expressed in cultured mammalian

* This work was supported in part by National Institutes of Health Grants DK32753 (to W. B. G.) and HL33991, HL48268, and EY11239 (to P. A.), a grant from Human Frontier Science Program Organization (to E. B. and P. A.), Deutsche Forschungsgemeinschaft Grant Be2253/1-1 (to E. B.), a grant from the American Heart Association (to M. Y.), and a grant from Itoh Foundation U.S.A. (to M. Y.). The costs of publication of this article were defrayed in part by the payment of page charges. This article must therefore be hereby marked "*advertisement*" in accordance with 18 U.S.C. Section 1734 solely to indicate this fact.

§ Contributed equally to this work.

‖ Present address: Pharmazeutische Chemie, Abtlg. Pharm. Biochemie, Universität Tübingen, Auf der Morgenstelle 8, D-72076 Tübingen, Germany.

§§ To whom correspondence should be addressed: Dept. of Pediatrics and Biological Chemistry, Johns Hopkins University School of Medicine, 420 Physiology Bldg., 725 N. Wolfe St., Baltimore, MD 21205-2185. Tel.: 410-955-3154; Fax: 410-955-3149; E-mail: myasui@jhmi.edu.

[1] The abbreviations used are: AQP, aquaporin; GFP, green fluorescent protein; HEK, human embryonic kidney; DIDS, 4,4′-diisothiocyanostilbene-2,2′-disulfonic acid; MES, 4-morpholineethanesulfonic acid; I-V, current-voltage; GABA, γ-aminobutyric acid; wt, wild-type.

renal cells. Our previous studies were restricted to expression in *X. laevis* oocytes (3, 12), because AQP6 was retained in intracellular membranes when expressed in cultured mammalian cells. Here we found that tagging the N terminus of AQP6 with GFP redirected its expression to the plasma membrane of cultured mammalian cells where the protein was amenable to electrophysiological analysis. These studies revealed unique selectivity for the nitrate anion, even without activation by acidic pH or Hg^{2+}. Nitrate selectivity was in part determined by a single residue of the aquaporin aqueous pore, threonine 63. Also, anomalous mole-fraction behavior was not observed with NO_3^-/Cl^- mixtures, indicating the presence of a single anion-binding site in each pore. Taken together, we propose that AQP6 may function as an intracellular vesicle nitrate channel and provide a model that explains how nitrate ions may pass through AQP6, based on the atomic structures of AQP1 and the ClC chloride channel.

MATERIALS AND METHODS

Cell Culture and Transfection—Human embryonic kidney cells (HEK293; ATCC) were maintained in Dulbecco's modified Eagle's medium:F-12 (1:1), penicillin, streptomycin, and 10% fetal calf serum. Transient transfections were performed with LipofectAMINE2000 reagent (Invitrogen) according to the manufacturer's instructions. Cells were treated with 2–4 μg of AQP6 plasmid DNA in a 35-mm well.

Confocal Microscopy—Cells were plated on glass coverslips 1 day post-transfection and then fixed in 4% paraformaldehyde the next day. Coverslips were mounted and observed under an LSM 410 confocal microscope (Zeiss).

Whole Cell Patch Clamp Recordings—Conventional tight seal whole cell recordings were performed at room temperature on HEK293 cells grown on glass coverslips 2 to 3 days post-transfection. Transfected cells expressing GFP were identified under a fluorescent microscope (TE200; Nikon). Cells were perfused with an extracellular solution (ES) containing the following (in mM): 150 NaCl, 1 $MgCl_2$, 1 $CaCl_2$, 40 sucrose, 0.1 niflumic acid, 0.1 4,4′-diisothiocyanostilbene-2,2′-disulfonic acid (DIDS), and 10 Hepes (pH 7.4 with Tris). Sucrose, niflumic acid, and DIDS were used to prevent the activation of endogeneous currents. The pipette solution contained the following (in mM): 150 CsCl, 0.2 EGTA, 10 Hepes (pH 7.4 with Tris). Acid solutions (pH 4–6.1) were made by substituting 10 mM MES for Hepes in ES without niflumic acid and DIDS and were puff-applied using a nearby pipette of 30–35-μm diameter. We tested solutions below pH 4 (pH 3.7). These solutions were made by adding gluconic acid to the solution containing MES, because we have observed that acid-induced AQP6 channel is impermeable to the gluconate (3). For the ion selectivity experiments, 150 mM NaCl in ES without niflumic acid and DIDS was replaced with 150 mM $NaNO_3$, 150 mM NaI, 150 mM NaBr, 150 mM NMDGCl, and 100 mM Na_2SO_4 or 100 mM $CaCl_2$ at both pH 7.4 and pH 4. In preliminary experiments, replacement of NaCl solution with these solutions at both pH 7.4 and pH 4 induced negligible conductance changes in control GFP-expressing cells (<0.6 nS). pClamp8 software (Axon Instruments) was used to sample and analyze data. The input capacitance was estimated from the decay time course of the capacitative surge, and this value was used to normalize the current amplitude and the conductance. Current-voltage (I-V) relationships were obtained at 100 ms of each voltage step from a holding potential of 0 or −40 mV. Conductance was calculated from the slope of the I-V relationship between reversal potential and reversal potential +40 mV. Junction potential correction was performed as described previously (15).

Data Analysis—Based on the reversal potentials, the relative ion permeability for monovalent ions was calculated according to the modified Goldman-Hodgkin-Katz equation, and that for divalent ions was calculating according to the equation of Fatt and Ginsborg (16).

The specific activation of AQP6 by low pH was characterized by fitting (by least squares) a Hill equation to the relationship between the corrected conductance ($G = G_{measured} - G_{nonspecific}$) and $[H^+]$: $G = G_{max}/(EC_{50}{}^n/[H^+]^n + 1)$, where n is the Hill coefficient, EC_{50} is the concentration of half-activation, and G_{max} is the corrected maximum conductance.

Computer Modeling of AQP6 Nitrate Ion Binding—Using Swiss PDB Viewer, a nitrate ion (from atomic resolution PDB coordinates 3LZT) was manually placed in the putative anion-binding site of a previously generated homology model of rat aquaporin-6 (12) in such a way to maximize favorable ligand-protein interactions (17). Key amino acid residues and structural features were visualized with VMD and Raster3D (18, 19).

RESULTS

Plasma Membrane Expression of GFP-AQP6—AQP6 is abundant in intracellular vesicles of acid-secreting type-A intercalated cells in renal collecting duct (2). When transfected into mammalian cell lines (Chinese hamster ovary, Madin-Darby canine kidney, or HEK293), rat AQP6 is also restricted to intracellular sites with no detectable expression in the plasma membranes (3). The intracellular location has prevented electrophysiological studies of AQP6 expressed in mammalian cells. To examine molecular mechanisms by which AQP6 is targeted to membrane compartments, AQP6 was tagged with GFP at either the N terminus (GFP-AQP6) or the C terminus (AQP6-GFP). HEK293 cells were then transfected with the DNA constructs, and the subcellular distribution of the expressed proteins was determined by confocal microscopy. As expected, GFP by itself is diffusely present throughout the cytosol (Fig. 1*A*). In contrast, GFP-AQP6 is exclusively present in the plasma membrane (Fig. 1*B*), whereas AQP6-GFP resides at intracellular sites in a reticular web-like pattern (Fig. 1*C*).

Characterization of AQP6: an Acidic pH-activated Channel—When over-expressed in *X. laevis* oocytes, AQP6 is expressed in the plasma membrane where permeation by ions occurs in response to acidic pH or Hg^{2+} (3). To further validate these findings, whole cell currents were measured in HEK293 mammalian cells transfected with GFP, GFP-AQP6 or AQP6-GFP. At pH 4, currents are rapidly and reversibly activated in cells expressing GFP-AQP6, but not in cells expressing GFP or AQP6-GFP (Fig. 2). The I-V relationship rectifies slightly in the inward direction, and the reversal potential is near 10 mV (see Fig. 2*E* and Table I). These features of acid-induced currents in cells expressing GFP-AQP6 are similar to measurements of AQP6 overexpressed in *X. laevis* oocytes (3). Moreover, when oocytes expressing GFP-AQP6 were examined, the protein behaved identically to wild-type AQP6 (data not shown).

At pH 6.1 the current responses were negligible, but marked activation of currents were observed in HEK293 cells expressing GFP-AQP6 at pH 5.6 or below (Fig. 3*A*). Attempts to measure currents at pH 3.7 or below were complicated by the appearance of nonspecific leak currents in control cells expressing GFP (Fig. 3*A*, *open circles*). Therefore, the AQP6-specific currents were calculated by subtracting the currents measured from control cells expressing GFP in solutions of corresponding pH values. After normalization to maximum currents (pH 4.1), the $[H^+]$-response relationship was fitted to the Hill equation, resulting in an EC_{50} value of 6.3 μM (pH 5.2) and a Hill coefficient of 1.04 (Fig. 3*B*).

Unique Anion Selectivity of AQP6: High Permeability to Nitrate—To estimate the ion selectivity of the AQP6 channel, current responses to voltage steps were measured first in a solution containing NaCl at pH 7.4 and then in solutions containing different ions. Shifts in reversal potential in substitution experiments were used to calculate the relative permeability to various ions (Table I). AQP6 currents exhibit substantial anion permeability (see Fig. 4 and Table I). In cells expressing GFP-AQP6, outward-rectifying currents were observed at pH 7.4 with a notable negative shift of the reversal potential immediately after replacement of the solution containing NaCl with $NaNO_3$ (Fig. 4, *A* and *C*). These data suggest that there is some basal channel activity of AQP6 channels at pH 7.4. At pH 4 the amplitudes of the outward currents are enhanced, with a −67-mV shift in reversal potential in a solution containing $NaNO_3$ (Fig. 4*D*). The calculated P_{NO_3}/P_{Cl} at pH 4 is 14.7 (see Fig. 4, *B* and *D*, and see Table I), similar to the high perm selectivity to NO_3^- at pH 7.4 (Table I). These observations

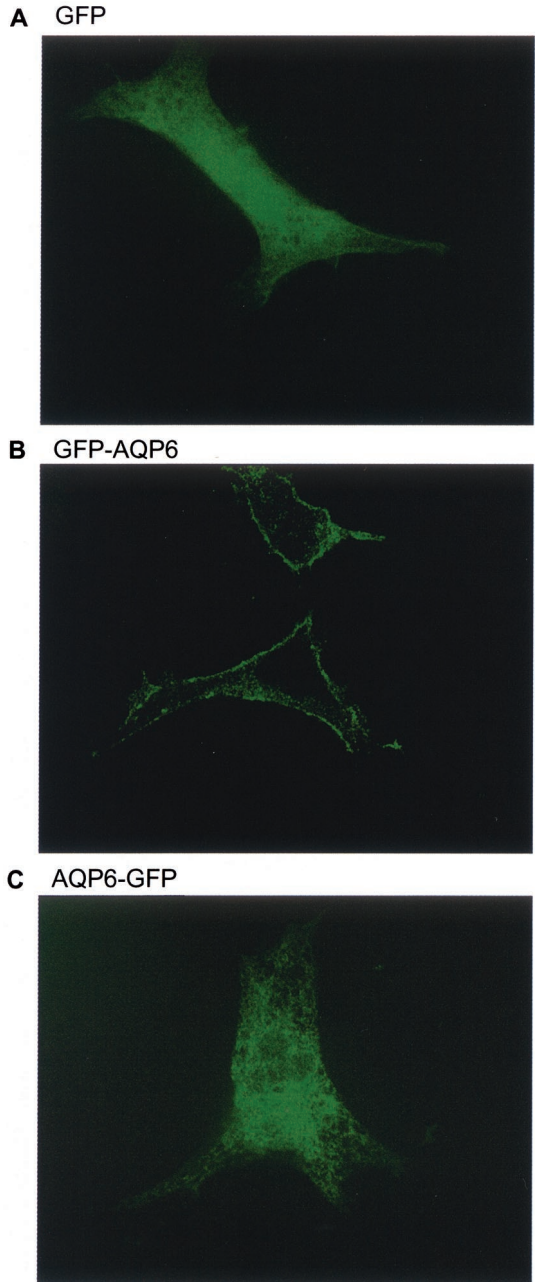

FIG. 1. **Plasma membrane expression of GFP-AQP6.** Confocal images of HEK293 cells transfected with GFP (*A*), GFP-AQP6 (*B*), or AQP6-GFP (*C*) (Nikon CF-Fluor objective, ×100, 1.4 of numerical aperture).

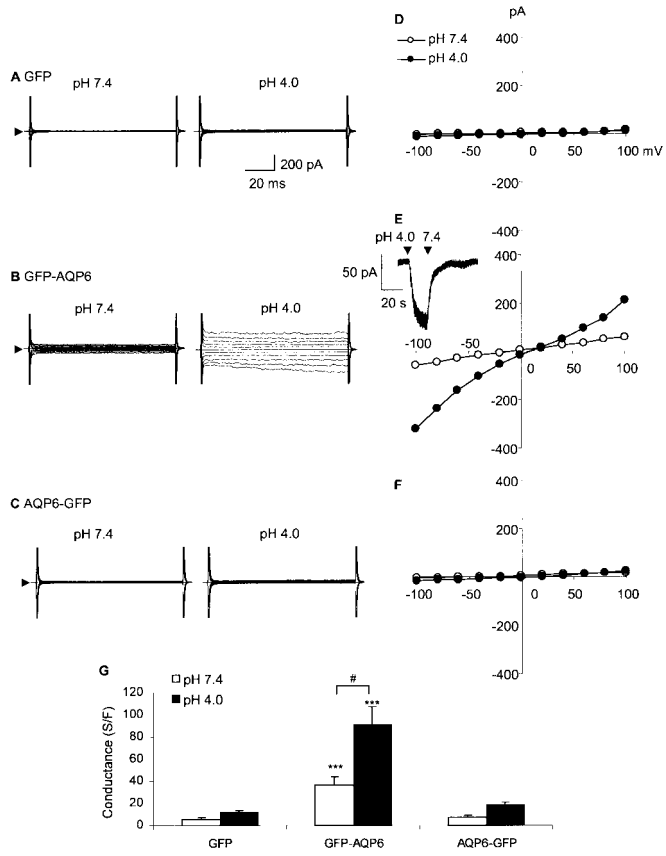

FIG. 2. **Acid-induced (pH 4) currents in HEK293 cells transfected with GFP (*A*), GFP-AQP6 (*B*), or AQP6-GFP (*C*).** Typical recordings in which application of acid solution evoked currents, and the relationships of the steady-state current to membrane voltage, are shown (*D–F*). The cell was held at 0 mV, and 100-ms voltage steps were applied (from −100 through +100 mV at increments of 20 mV). *Open circles* indicate basal currents, and *closed circles* indicate acid-stimulated currents. The *inset* (*E*) shows a continuous current record of a GFP-AQP6-expressing cell held at −40 mV. At the indicated points, the solution was changed from pH 7.4 to pH 4 and back. The *bar graph* (*G*) summarizes the ionic conductance before (*open column*) and 15–20 s after (*solid*) switching to acid (pH 4) bath solution. Conductance was calculated from the slope of the I-V curve in the interval between the experimental reversal potential and the reversal potential + 40 mV. Values are presented as mean ± S.E. (n = 6 in GFP, n = 7 in GFP-AQP6, and n = 6 in AQP6-GFP). The significance level of $p < 0.001$ (***) was achieved when compared with GFP-expressing cells. The significance level of $p < 0.05$ (#) was achieved when tested before and after switching to acid bath solution in GFP-AQP6-expressing cells.

indicate that NO_3^- is much more permeable than Cl^- both at acid pH and at neutral pH. A similar nitrate permeability was found when wild-type AQP6 is expressed in oocytes (not shown). A series of ion substitution experiments gave the following halide permeability sequence: $NO_3^- \gg I^- \gg Br^- > Cl^-$ (Table I). In contrast to monovalent anions, an inward-rectifying current with a positive reversal potential was observed in a solution containing Na_2SO_4 at pH 4 (Table I), suggesting a lower permeability of SO_4^{2-} in AQP6 channels (P_{SO4}/P_{Cl} of 0.01 ± 0.05 at pH 4). Cation permeability was also examined. Replacing extracellular Na^+ with $NMDG^+$ did not shift the reversal potential, suggesting that the acid-induced AQP6 currents were not cation-permeable (Table I). On changing to a solution containing $CaCl_2$ at pH 4, no potentiation of inward currents was observed, and there was even slight negative shift of reversal potential, suggesting that the channel was virtually impermeable to Ca^{2+} (Table I).

Identification of the Pore Residues by Site-directed Mutagenesis—To identify structures involved in anion-binding site for AQP6, we used site-directed mutagenesis followed by electrophysiological assessment based on the information provided by AQP1 and ClC structures. Sequence alignments of mammalian aquaporins revealed that AQP6 has several unique hydrophilic or charged residues in the pore region: Tyr-34, Thr-58, Thr-63, and Lys-72 (Fig. 5*A*). These residues are identical in AQP6 orthologs from rats, mice, monkeys, and humans but are not found in other known aquaporins. Cells expressing the GFP-AQP6 mutant polypeptide T58A behaved the same as cells expressing wild-type GFP-AQP6 to acidic pH and Hg^{2+}, except the maximum current level was smaller than that in wild-type GFP-AQP6 (data not shown). GFP-AQP6 mutant polypeptide K72E did not traffic to the plasma membranes when transfected into HEK293 cells, and mutant polypeptide Y34F did not even traffic to the plasma membrane of *Xenopus* oocytes (data not shown).

TABLE I
Reversal potentials (Erev), reversal potential shifts (ΔErev), and permeability ratios for AOP6

	n	Erev at pH 7.4	Erev at pH 4	ΔErev at pH 7.4	ΔErev at pH 4	P_X/P_{Cl} at pH 7.4	P_X/P_{Cl} at pH 4
		mV	*mV*	*mV*	*mV*		
NaCl	60	−9.9 ± 1.1	9.5 ± 0.7	0	0	1.0	1.0
$NaNO_3$	10	−63.0 ± 4.3	−60.5 ± 2.6	−55.7 ± 3.7	−67.1 ± 2.5	9.8 ± 1.4 (P_{NO3}/P_{Cl})	14.7 ± 1.7 (P_{NO3}/P_{Cl})
NaI	3 (pH 7.4) 7 (pH 4)	−41.0 ± 14.5	−33.6 ± 4.8	−23.7 ± 11.4	−48.6 ± 2.4	3.1 ± 1.4 (P_I/P_{Cl})	7.0 ± 0.7 P_I/P_{Cl})
NaBr	5 (pH 7.4) 11 (pH 4)	−6.0 ± 1.2	−4.5 ± 1.4	−4.4 ± 0.7	−13.4 ± 1.0	1.2 ± 0.03 (P_{Br}/P_{Cl})	1.7 ± 0.07 (P_{Br}/P_{Cl})
Na_2SO_4	4	3.3 ± 0.9	34.3 ± 5.3	12.3 ± 4.5	23.0 ± 5.6		
NMDGCI	4	−7.0 ± 2.5	16.1 ± 1.7	0.3 ± 4.8	2.5 ± 0.6		
$CaCl_2$	4	−3.0 ± 1.7	7.5 ± 0.9	2.0 ± 1.4	−6.8 ± 1.0		

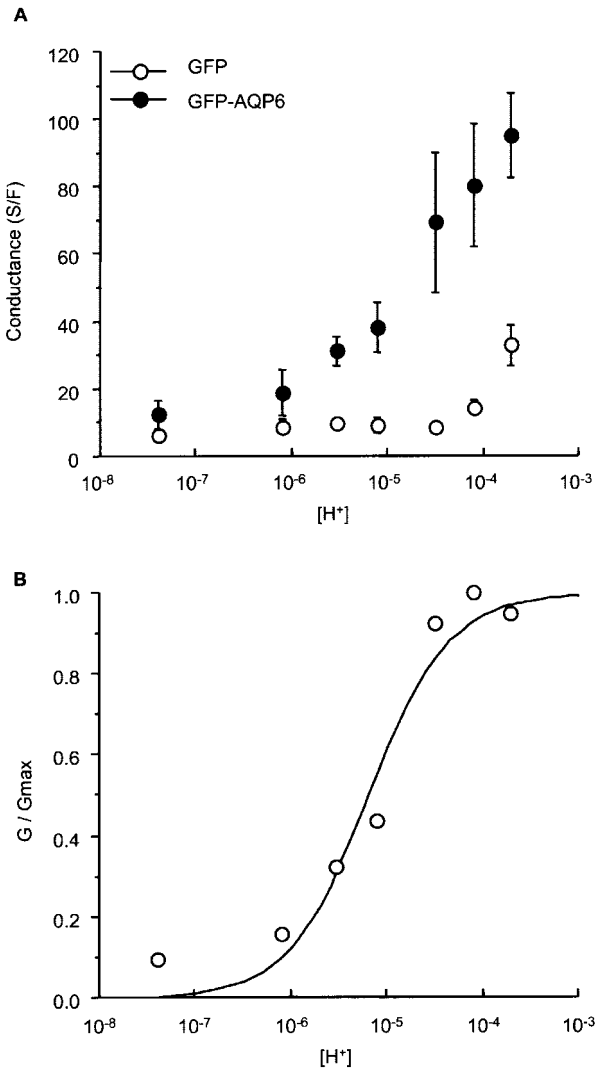

FIG. 3. **Relationship between AQP6 ion conductance and extracellular proton concentration.** Ion conductance (*A*) of cells transfected with GFP (*open circles*) or GFP-AQP6 (*solid circles*) was measured in solutions of various pH. Values represent the mean ± S.E. (n = 5–9). Normalized conductances (*B*) were calculated as the ratio of the corrected conductance ($G_{measured} - G_{nonspecific}$) and the maximum conductance (pH 4.1), plotted against the logarithmic scale of external proton concentration ($[H^+]$) and fitted to the Hill equation (*solid line*).

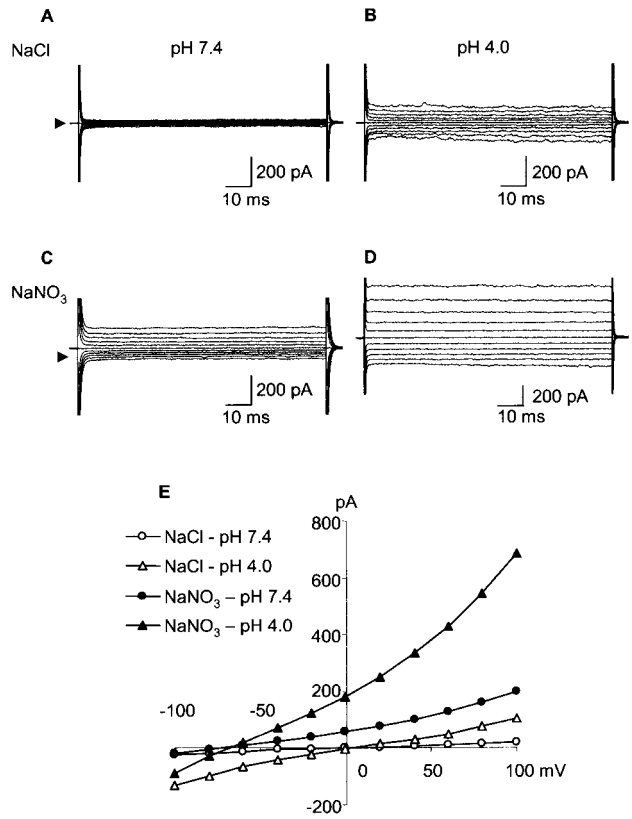

FIG. 4. **Current responses induced by the replacement of Cl^- with NO_3^- in GFP-AQP6-expressing cells.** Typical recordings of currents from the same GFP-AQP6-expressing cell in NaCl solution (*A* and *B*) and $NaNO_3$ solution (*C* and *D*) at pH 7.4 (*left traces*) and pH 4 (*right traces*) are shown. The *arrowhead* indicates the zero current level. The corresponding I-V relationships are depicted in *E*. Representative traces of 10 experiments were shown.

The currents in response to acidic pH are significantly greater in cells expressing the GFP-AQP6 mutant polypeptide T63I than in cells expressing wild-type GFP-AQP6, although the two cell types exhibited fairly similar responses to Hg^{2+} (Fig. 5*B*). The response to different proton concentrations in cells expressing the GFP-AQP6 mutant polypeptide T63I gave an EC_{50} value of 8.8 μM (pH 5.1) and a corresponding Hill coefficient of 1.02, close to the values in cells expressing wild-type GFP-AQP6 (Fig. 5, *C* and *D*). Thus, the pH sensitivity of the T63I mutant remains unchanged, suggesting that Thr-63 is unlikely to play a role as a pH sensor but is an important site for ion permeability.

Membrane currents of cells expressing the GFP-AQP6 mutant polypeptide T63I were examined using NaCl and $NaNO_3$ solutions at pH 7.4 and 4.0. In a solution containing NaCl at pH 7.4, small currents are observed (Fig. 6*A*) with a reversal potential of −4.0 ± 0.7 mV (n = 6), which is slightly more positive than that of wild-type GFP-AQP6. At pH 4, the current amplitudes are drastically enhanced (Fig. 6*B*) compared with pH 7.4 (Fig. 6*A*), and the reversal potential was 6.9 ± 0.5 mV similar to that observed in cells expressing wild-type GFP-AQP6 (Table I). The increase in current amplitude between pH 7.4 and

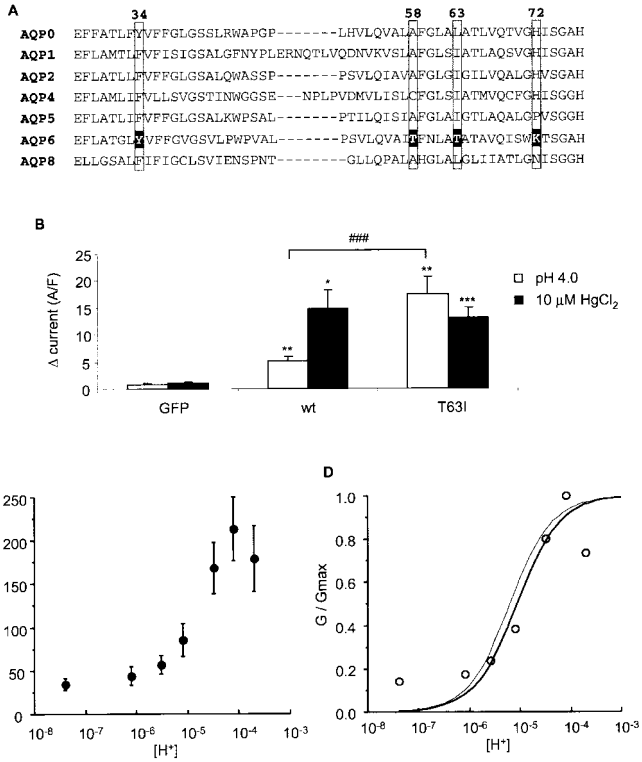

FIG. 5. **Current responses in T63I mutant.** *A*, amino acid sequence alignment of rat aquaporins indicating several unique residues in AQP6. *B*, cells transiently transfected with GFP, GFP-AQP6 (*wt*), or GFP-T63I-AQP6 (*T63I*), were challenged with acid solution (at pH 4) or $HgCl_2$ (10 μM) at a holding potential of −40 mV. The *bar graph* shows the current density 15–20 or 80 s after the application of acid (*open column*) or $HgCl_2$ (*solid column*). Values are presented as mean ± S.E. (n = 5 for GFP, n = 10 for wt, and n = 8 for T63I). Significance levels are represented for $p < 0.05$ (*), $p < 0.01$ (**), and $p < 0.001$ (***) compared with GFP-expressing cells. The significance level of $p < 0.001$ (###) was achieved when wt and T63I were compared. *C*, the relationship between ion conductance is compared with the extracellular proton concentration for the T63I mutant. Values represent mean ± S.E. *D*, after subtraction and normalization to the maximum conductance (at pH 4.1), the relationship was fitted by the Hill equation (*solid line*). The *thin line* indicates the relationship of the wt AQP6 from Fig. 3.

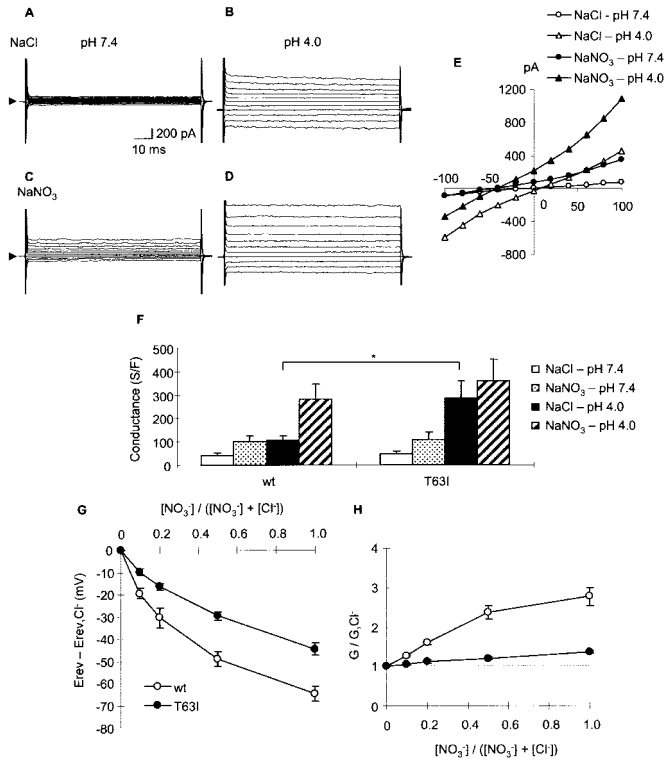

FIG. 6. **NO_3^- current in T63I mutant.** Representative currents from the same GFP-T63I-AQP6-expressing cell in NaCl solution (*A* and *B*) and $NaNO_3$ solution (*C* and *D*) at pH 7.4 (*left traces*) and pH 4 (*right traces*) are shown. The *arrowhead* indicates the zero current level. The corresponding I-V relationships are depicted in *E*. The *bar graph* (*F*) shows the conductance in NaCl solution (pH 7.4, *open column*; pH 4, *solid column*) and $NaNO_3$ solution (pH 7.4, *hatched column*; pH 4, *diagonal column*). The conductance was calculated from the slope of the I-V relationship in the same batches of cells transfected with wt or T63I. Values represent mean ± S.E. (n = 6). A significance level of $p < 0.05$ (*) was achieved when compared with wt. The relationship between the deviation from reversal potential of Cl^- ($Erev - Erev,Cl^-$ in *G*) or conductance relative to Cl^- conductance ($G/G,Cl^-$ in *H*) and mole-fraction of NO_3^- in wt (*open circles*) and T63I (*solid circles*) at pH 4 are shown. Values are mean ± S.E. (n = 4).

4.0 is obviously greater for the mutant (Fig. 6, *A* and *B*) than that observed for wild-type (Fig. 4, *A* and *B*). In a solution containing $NaNO_3$, outward currents measured at pH 7.4 (Fig. 6*C*) were higher compared with those observed with an NaCl-rich solution (Fig. 6*A*), with a mean reversal potential of −44.7 ± 3.6 mV. In a solution containing $NaNO_3$, currents measured at pH 4 (Fig. 6*D*) were higher compared with those observed in a solution containing $NaNO_3$ at pH 7.4. The mean reversal potential measured in the $NaNO_3$-rich solution at pH 4 was −37.8 ± 1.6 mV. Summarized data are presented in Fig. 6*F*, which depicts whole cell membrane conductance. The major effect of the T63I mutation is a significantly enhanced conductance in solutions containing NaCl at pH 4 compared with that of wild-type. In contrast, this mutation did not significantly alter the conductance in solutions containing NaCl at pH 7.4 or $NaNO_3$ at pH 4 or pH 7.4, when compared with the wild-type channel (Fig. 6*F*). Relative permeability ratios (P_{NO_3}/P_{Cl}) calculated from the mean values of shifts in reversal potential are 5.2 at pH 7.4 (5.2 ± 0.7, n = 6) and 5.9 at pH 4 (Table II). Both values are lower than those of wild-type GFP-AQP6, which are 9.8 and 14.7 (Table I), respectively, suggesting a somewhat lower selectivity of the mutant channel.

To further determine the halide permeability in the GFP-AQP6 mutant polypeptide T63I, we also measured reversal potentials in solutions containing NaI or NaBr at pH 4. Shifts

TABLE II
Reversal potential shifts (ΔErev) and permeability ratios at pH 4 for T63I mutant

	n	ΔErev at pH 4	P_X/P_{Cl} at pH 4
		mV	
$NaNO_3$	6	−44.7 ± 1.9	5.9 ± 0.4 (P_{NO3}/P_{Cl})
NaI	4	−40.8 ± 1.6	5.0 ± 0.3 (P_I/P_{Cl})
NaBr	5	−14.4 ± 1.1	1.8 ± 0.08 (P_{Br}/P_{Cl})

in reversal potentials at pH 4 are summarized in Table II. For the mutant channel, the permeability ratio of P_I/P_{Cl} was 5.0, and that of P_{Br}/P_{Cl} was 1.8. Thus, T63I still has a halide permeability sequence of $NO_3^- > I^- > Br^- > Cl^-$ similar to that of wild-type, but the relatively lower permeability ratios for P_{NO3}/P_{Cl} and P_I/P_{Cl} again suggest that the mutant channel has a somewhat lower selectivity.

Movement of Ions through the Pore—If an ion channel holds one ion at a time when two permeant ions are mixed together at different concentration ratios, membrane conductance and reversal potential will change monotonically. In contrast, in multi-ion pore models, membrane conductance and reversal potential go through a minimum or maximum as a function of the concentration ratio of two permeant ionic species, a phenomenon commonly referred to as anomalous mole-fraction (20). Cells expressing wild-type GFP-AQP6 were evaluated, but membrane conductance and a shift in reversal potential

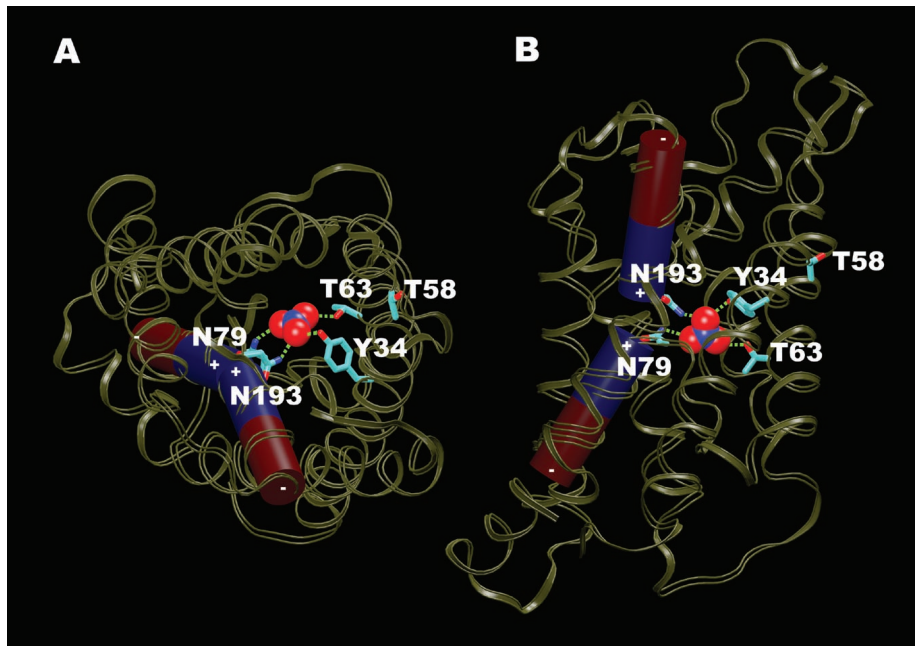

FIG. 7. **A comparison-based structural model suggests that nitrate ions traverse the aqueous pathway through each subunit of the AQP6 tetramer.** The nitrate ion is depicted with van der Waals space-filling spheres and is predicted to traverse through the center of each subunit. *A* and *B*, top and side views of a single subunit of AQP6. Partial helical dipoles are shown as *cylinders*. These segments meet in the center of the monomer and are predicted to form a partially positively charged environment suitable for anion binding. Unlike other aquaporins, AQP6 contains hydroxyl-containing residues (*T63* and *Y34*) that are analogous to anion-coordinating residues in ClC (*S107* and *Y445*). Thr-58 (*T58*), however, does not appear to participate in nitrate binding. The amide nitrogens of the Asn residues in the Asn-Pro-Ala motifs (*N79* and *N193*) may contribute to a nitrate-binding site, in a fashion analogous to backbone amide nitrogens of the chloride channel (Ile-356 and Phe-357). The pathway through the center of the tetramer of AQP6, on the other hand, does not contain prominent features suggestive of anion transport.

changed monotonically when the concentration ratio between solutions containing NaCl and $NaNO_3$ at pH 4 was varied (Fig. 6, *G* and *H*). Likewise, anomalous mole-fraction behavior was not observed with Cl^-/Br^- or with Cl^-/I^- mixtures (data not shown). These observations suggest that GFP-AQP6 may have a single ion-binding site. Moreover, anomalous mole-fraction behavior was not observed with NO_3^-/Cl^- (Fig. 6, *G* and *H*), Cl^-/Br^-, or Cl^-/I^- mixtures (data not shown) in T63I mutant, suggesting that T63I may also have a single ion-binding site similar to wild-type.

DISCUSSION

The closest sequence-related homologs of mammalian AQP6 are AQP0 (lens fibers), AQP2 (collecting duct principal cells), and AQP5 (secretory glands); however AQP6 exhibits markedly different cellular properties. Whereas the other aquaporins are known to reside in the plasma membrane (AQP0 and AQP5) or traffic to the plasma membrane (AQP2), AQP6 is restricted to intracellular locations. Our studies with the GFP-AQP6 implicate the N terminus of AQP6 as a determinant of this distribution. Unlike other the aquaporins, rapid and reversible anion conductance was revealed when GFP-AQP6 is expressed in the plasma membrane of mammalian cells (HEK293). In addition, surprisingly high permeation by NO_3^- was identified and found to require a single pore-lining threonine. Together these observations indicate that the primary biological function of AQP6 is not water transport. In contrast, we consider it likely that AQP6 may regulate an intracellular process within type-A intercalated cells of collecting duct.

Intracellular Localization of AQP6—In our earlier immunogold electron microscopic studies, we reported that AQP6 is almost exclusively localized in intracellular vesicles containing H^+-ATPase but is absent from the plasma membrane (2, 3). Attempts to express AQP6 in mammalian epithelial cells by transient transfection with rat AQP6 cDNA revealed that the protein remains in intracellular sites, precluding electrophysiological analyses of AQP6 in mammalian cells. Here we found that the addition of the GFP tag to the N terminus, but not the C terminus, causes AQP6 to traffic to the plasma membrane. This suggests that not C terminus but N terminus of AQP6 is important for the restriction of AQP6 to intracellular sites. The GFP tag may interfere with the recognition of the signal in the N-terminal AQP6 by the proteins that determine AQP6 trafficking. Delineation of the specific determinants required for membrane trafficking is now being pursued with a series of deletions and point mutations at the N terminus of AQP6.

Acid-activated Anion Channel—Electrophysiological assessment of GFP-AQP6 in HEK293 mammalian cells demonstrated rapid and reversible activation of AQP6 by low pH. The $[H^+]$-response relationship (pH 3.7–7.4) gave an EC_{50} value of 6.3 μM (pH 5.2) and a Hill coefficient of 1.04. Low pH extremes are physiologically relevant, because AQP6 colocalizes with H^+-ATPase in intracellular vesicles of acid-secreting type-A intercalated cells where the pH drops to 5.0 or lower (21). The Hill coefficient of 1.04 suggests that the binding of a proton to a single site fully activates the channel. The response to extracellular pH of AQP6 is similar to that of ClC-2 chloride channel, although its anion selectivity is different: $Cl^- = NO_3^-$ for ClC-2 (22, 23). While the amino acid Glu-419 was identified in the extracellular region as the pH sensor in ClC-2 (22), the identity of the pH sensor of AQP6 is still being sought.

Is AQP6 a Nitrate Channel?—The explanation of why AQP6 acts as an acid-induced anion channel in type-A intercalated cells in collecting duct is beginning to emerge. AQP6 is unlike other known anion channels. First, a series of substitution experiments indicated that AQP6 has an anion permeability sequence of $NO_3^- \gg I^- \gg Br^- > Cl^- > SO_4^{2}$. This order resembles that of the GABA- and glycine-gated channels (19). However, selectivity for nitrate by AQP6 is considerably higher than that of GABA- or glycine-gated channels: $P_{NO3}/P_{Cl} > 9.8$ (AQP6) and ~2 (GABA- or glycine-gated channels). Moreover, our data suggest that AQP6 has a single ion-binding pore; GABA- or glycine-gated channels have been proposed to contain a multi-ion-binding pore. Second, high permeability for nitrate is observed even at pH 7.4. This implies either that the channel is already open to some extent even under basal conditions, or permeation by nitrate induces channel gating. Third, AQP6 is not inhibited by known anion channel inhibitors such as DIDS, 5-nitro-2-(3-phenylpropylamino) benzoic acid (NPPB), niflumic acid, and diphenylamine-2-carboxylic acid (DPC) (3). Interestingly, the permeability sequence is identical to that of lysosomal membranes (25). The acidic pH within the interior of lysosomes is generated and maintained

by a V-type H^+-ATPase, which is an electrogenic process (26), and anion conductance is needed to maintain electroneutrality across the membranes (27). Similar mechanisms may take place in intracellular vesicles where H^+-ATPase and AQP6 colocalize within acid-secreting type-A intercalated cells of renal collecting duct. Note that the osmotic water permeability of AQP6-expressing oocytes was not altered by the presence of nitrate ions in the extracellular solution, suggesting that AQP6 may function as a nitrate channel rather than as a water channel.[2]

The physiological relevance of the high permeability of AQP6 by nitrate needs to be established. Intracellular nitric oxide is produced by nitric-oxide synthase in response to various stimuli and is rapidly metabolized into nitrate. In renal collecting duct, nitric oxide has been reported to inhibit H^+-ATPase activity in microdissected, isolated tubules or in an *in vivo* ureteral obstruction model (28, 29). Nitrate has also been reported to inhibit H^+-ATPase (30). Although an interaction between AQP6 and H^+-ATPase activity has yet to be elucidated, AQP6 may be involved in the regulation of H^+-ATPase activity in acid-secreting type-A intercalated cells. We recently generated AQP6 null mice by homologous recombination,[3] and these animals may be useful to examine whether AQP6 is involved in regulation of H^+-ATPase activity by nitric oxide signaling.

Identification of the Pore for Nitrate—Our electrophysiological measurements indicate that the pore-lining residue Thr-63 in AQP6 is required for nitrate selectivity. Our data also suggest a single ion-binding pore in each subunit with monotonic mole-fraction behavior with NO_3^-/Cl^- mixtures. The high permeability to nitrate and the single ion-binding pore for AQP6 can be explained by structural assessment. Using the AQP1 crystal structure as a template (8), we recently built a three-dimensional structural model of AQP6 (12). One of the water-binding sites for AQP1 is present at the midpoint of the pore where the N termini of short pore α-helices meet to induce a positive electric field (6). The AQP6 model was useful in illustrating that the same site is where nitrate binding may occur (Fig. 7). AQP6 contains hydroxyl-containing residues (Tyr-34 and Thr-63) on the channel wall opposite the two highly conserved asparagine residues (Asn-79 and Asn-193) and a nitrate ion coordinates with these four residues (Fig. 7). Thr-63 is unique to AQP6, because all other aquaporins have hydrophobic residues at that site; however *Drosophila* Big Brain, a homolog recently reported to exhibit ion conductance (31), shares the residue corresponding to Tyr-34. Our attempts to substitute a phenylalanine for tyrosine in AQP6 were unsuccessful, because the mutant protein apparently failed to traffic to the plasma membrane (data not shown). The possible role of the other residues determining the nitrate specificity remains to be investigated.

Although ClC chloride channels do not belong to the aquaporin gene family, a similar mechanism for anion coordination was demonstrated in ClC chloride channel (32, 33). Like AQP1, ClC has a symmetrical hourglass shape with a constriction in the center of the membrane and wide openings at the membrane surfaces. In ClC, a positive electric field contributed by those short pore α-helices provides the favorable electrostatic environment for chloride with two hydrophilic residues at the constriction (Ser-107 and Tyr-445).

The pore of AQP1, and presumably all other aquaporins, is largely hydrophobic with water molecules spaced at four hydrophilic sites (8). This is indeed important for ultra high speed movement of water molecules through the pore (9–11). This fundamental structure of the pore also explains the anion permeability sequence through AQP6. The mobility sequence for the ions in aqueous solution is Br^- ($D = 2.08 \times 10^{-5}$ cm^2 s^{-1}) > I^- (2.04) > Cl^- (2.03) > NO_3^- (1.90) > SO_4^{2-} (1.06), where D represents the diffusion coefficient. Thus, the high P_{NO3}/P_{Cl} cannot be explained for AQP6 if the pore is entirely filled with water. The predicted AQP6 structure conforms well to the nitrate ion (Fig. 7), but the actual crystal structural model for AQP6 has not yet been reported.

Except a few unique amino acid residues such as Tyr-34 and Thr-63, the residues critical for water channel function are very well conserved in AQP6, suggesting that very subtle differences can lead to major differences in biophysical function. We believe that understanding structure-function relationships of AQP6 will provide fundamental and novel insights into new functions of aquaporins. We particularly hope to understand the molecular mechanisms behind the impermeability to ions observed for aquaporins in general, in contrast to the rapid transport of anions by AQP6.

Acknowledgments—We thank Fong Peying for a critical reading of the manuscript.

REFERENCES

1. Agre, P., King, L. S., Yasui, M., Guggino, W. B., Ottersen, O. P., Fujiyoshi, Y., Engel, A., and Nielsen, S. (2002) *J. Physiol.* **542,** 3–16
2. Yasui, M., Kwon, T. H., Knepper, M. A., Nielsen, S., and Agre, P. (1999) *Proc. Natl. Acad. Sci. U. S. A.* **96,** 5808–5813
3. Yasui, M., Hazama, A., Kwon, T. H., Nielsen, S., Guggino, W. B., and Agre, P. (1999) *Nature* **402,** 184–187
4. Promeneur, D., Kwon, T. H., Yasui, M., Kim, G. H., Frokiaer, J., Knepper, M. A., Agre, P., and Nielsen, S. (2000) *Am. J. Physiol.* **279,** F1014–F1026
5. Agre, P., Lee, M. D., Devidas, S., and Guggino, W. B. (1997) *Science* **275,** 1490
6. Murata, K., Mitsuoka, K., Hirai, T., Walz, T., Agre, P., Heymann, J. B., Engel, A., and Fujiyoshi, Y. (2000) *Nature* **407,** 599–605
7. Fu, D., Libson, A., Miercke, L. J., Weitzman, C., Nollert, P., Krucinski, J., and Stroud, R. M. (2000) *Science* **290,** 481–486
8. Sui, H., Han, B. G., Lee, J. K., Walian, P., and Jap, B. K. (2001) *Nature* **414,** 872–878
9. de Groot, B. L., and Grubmuller, H. (2001) *Science* **294,** 2353–2357
10. Tajkhorshid, E., Nollert, P., Jensen, M. O., Miercke, L. J., O'Connell, J., Stroud, R. M., and Schulten, K. (2002) *Science* **296,** 525–530
11. Kozono, D., Yasui, M., King, L. S., and Agre, P. (2002) *J. Clin. Invest.* **109,** 1395–1399
12. Hazama, A., Kozono, D., Guggino, W. B., Agre, P., and Yasui, M. (2002) *J. Biol. Chem.* **277,** 29224–29230
13. Anthony, T. L., Brooks, H. L., Boassa, D., Leonov, S., Yanochko, G. M., Regan, J. W., and Yool, A. J. (2000) *Mol. Pharmacol.* **57,** 576–588
14. Saparov, S. M., Kozono, D., Rothe, U., Agre, P., and Pohl, P. (2001) *J. Biol. Chem.* **276,** 31515–31520
15. Ikeda, M., Iyori, M., Yoshitomi, K., Hayashi, M., Imai, M., Saruta, T., and Kurokawa, K. (1993) *J. Membr. Biol.* **136,** 231–241
16. Fatt, P., and Ginsborg, B. L. (1958) *J. Physiol.* **142,** 516–543
17. Walsh, M. A., Schneider, T. R., Sieker, L. C., Dauter, Z., Lamzin, V. S., Wilson, K. S. (1998) *Acta Crystallogr. D Biol. Crystallogr.* **54,** 522–546
18. Humphrey, W., Dalke, A., and Schulten, K. (1996) *J. Mol. Graph.* **14,** 33–38
19. Merritt, E. A., and Bacon, D. J. (1997) *Methods Enzymol.* **277,** 505–524
20. Hagiwara, S., and Takahashi, K. (1974) *J. Membr. Biol.* **18,** 61–80
21. Glickman, J., Croen, K., Kelly, S., and Al Awqati, Q. (1983) *J. Cell Biol.* **97,** 1303–1308
22. Stroffekova, K., Kupert, E. Y., Malinowska, D. H., and Cuppoletti, J. (1998) *Am. J. Physiol.* **275,** C1113–C1123
23. Tewari, K. P., Malinowska, D. H., Sherry A. M., and Cuppoletti, J. (2000) *Am. J. Physiol.* **279,** C40–C50
24. Bormann, J., Hamill, O. P., and Sakmann, B. (1987) *J. Physiol.* **385,** 243–286
25. Klemm, A. R., Pell, K. L., Anderson, L. M., Andrew, C. L., and Lloyd, J. B. (1998) *Biochim. Biophys. Acta* **1373,** 17–26
26. Harikumar, P., and Reeves, J. P. (1983) *J. Biol. Chem.* **258,** 10403–10410
27. Schwartz, G. J., and Al Awqati, Q. (1986) *Ann. Rev. Physiol* **48,** 153–161
28. Tojo, A., Guzman, N. J., Garg, L. C., Tisher, C. C., and Madsen, K. M. (1994) *Am. J. Physiol.* **267,** F509–F515
29. Valles, P. G., and Manucha, W. A. (2000) *Kidney Int.* **58,** 1641–1651
30. Arai, H., Pink, S., and Forgac, M. (1989) *Biochemistry* **28,** 3075–3082
31. Yanochko, G. M., and Yool, A. J. (2002) *J. Neurosci.* **22,** 2530–2540
32. Dutzler, R., Campbell, E. B., Cadene, M., Chait, B. T., and MacKinnon, R. (2002) *Nature* **415,** 287–294
33. Jentsch, T. J. (2002) *Nature* **415,** 276–277

[2] Masato Yasui, unpublished data.
[3] Masato Yasui, unpublished data.